Available online at www.sciencedirect.com
ScienceDirect
Journal of Photochemistry and Photobiology A: Chemistry 183 (2006) 138–145
Journal of Photochemistry and Photobiology A:Chemistry
www.elsevier.com/locate/jphotochem

Mechanism of squarylium cyanine and $Ru(dcbpy)_2(NCS)_2$ co-sensitization of colloidal TiO_2

Ping Zuo [a], Chao Li [b], Yi-Shi Wu [a], Xi-Cheng Ai [a,*], Xue-Song Wang [b,*], Bao-Wen Zhang [b], Jian-Ping Zhang [a,*]

[a] *State Key Laboratory for Structural Chemistry of Unstable and Stable Species, Institute of Chemistry, Chinese Academy of Sciences, No. 2, 1st North Street, Zhongguancun, Beijing 100080, PR China*

[b] *Technical Institute of Physics and Chemistry, Chinese Academy of Sciences, Beijing 100101, PR China*

Received 26 October 2005; received in revised form 13 February 2006; accepted 5 March 2006
Available online 17 April 2006

Abstract

We have investigated the mechanism of squarylium cyanine (SQC) and $Ru(dcbpy)_2(NCS)_2$ (N3) co-sensitization of colloidal TiO_2 by means of time-resolved spectroscopies. Picosecond time-resolved fluorescence measurements combined with solvent–effect tests revealed a planar and a twisted conformer of the lowest singlet-excited state SQC (^{1}SQC*). Quenching of ^{1}SQC* fluorescence by adsorption on TiO_2 and further by co-adsorption with N3 was observed, which are ascribed to the ^{1}SQC*-to-TiO_2 and ^{1}SQC*-to-N3$^{\bullet+}$ electron transfer (ET) reactions based on femtosecond time-resolved absorption results. The planar and the twisted ^{1}SQC* conformers are able to inject electrons into the conduction band of TiO_2 with the rates of 1/2.76 ns^{-1} and 1/0.30 ns^{-1}, and to reduce N3$^{\bullet+}$ with the rates of 1/2.56 ns^{-1} and 1/0.28 ns^{-1}, respectively. The latter pair of rates are significantly larger than those of the $TiO_2(e^-)$-to-N3$^{\bullet+}$ back electron transfer (BET) reactions. In addition, ground state SQC is also found to be able to efficiently reduce N3$^{\bullet+}$ with a rate constant of 1/0.32 ns^{-1}. These results imply that minor amount of SQC as a co-adsorbate can effectively intercept the $TiO_2(e^-)$-to-N3$^{\bullet+}$ BET, a mechanism which accounts for the improvement of light-to-electricity conversion efficiency of dye-sensitized solar cells through N3 and SQC co-sensitization (D. Zhang et al., J. Photochem. Photobiol. A: Chem. 135 (2000) 235).

Keywords: Dye-sensitized semiconductor solar cell (DSSC); Squarylium cyanine; N3; TiO_2; Time-resolved spectroscopy

1. Introduction

The dye-sensitized nanocrystalline semiconductor solar cell (DSSC) developed by Grätzel and co-workers has been attracting extensive research interests owing to its high light-to-electrical energy conversion efficiency [1–4]. Practically, the DSSC device, which utilizes the porous nanocrystalline TiO_2 film sensitized by transition metal complex $Ru(dcbpy)_2(NCS)_2$ [dcbpy = 4,4′-dicarboxy-2,2′-bipyridine] (N3) as the working electrode, achieves a conversion efficiency as high as ∼10% [4,5].

Time-resolved spectroscopies have been widely used in characterizing the dye–TiO_2 interfacial carrier dynamics, and have established that N3 injects electrons from its electronically excited states into the conduction band of TiO_2 nanocrystals with a quantum efficiency close to unity [6]. These forward electron transfer (ET) reactions proceed on a few tens of femtoseconds and a few picoseconds, respectively, from the singlet and triplet metal-to-ligand charge transfer states ^{1}MLCT* and ^{3}MLCT* [7–11], whereas the back electron transfer (BET) from the conduction band $TiO_2(e^-)$ to the one-electron oxidized N3 (N3$^{\bullet+}$) is much slower, i.e. on the timescales of submicroseconds to milliseconds [2,6,8]. It is generally accepted that an excellent electric contact between the π*-electron orbital of bipyridine ligand and the vacant $3d^0$ orbital of Ti^{4+}, bridged by the carboxyl group, provides the structural basis for the extremely efficient ET reactions, and that the unique redox property of N3/N3$^{\bullet+}$ ensures an extremely large forward-to-backward ET ratio [12,13]. In addition to the above kinetic advantages of the TiO_2–N3 system, the light harvester N3 exhibits broad optical absorption in the entire visible spectral range with a weaker extension into the near-infrared region.

Despite the high light-to-electrical energy conversion efficiency, the action spectrum of N3-sensitized DSSC does not

* Corresponding authors. Tel.: +86 10 82616163; fax: +86 10 82616163.
E-mail address: jpzhang@mail.iccas.ac.cn (J.-P. Zhang).

1010-6030/$ – see front matter © 2006 Elsevier B.V. All rights reserved.
doi:10.1016/j.jphotochem.2006.03.007

fully match the solar spectrum, and the efficiency of light harvesting is limited by the poor molar extinction coefficient of N3 (14,200 M^{-1} cm^{-1} at 534 nm for maximum [6]). To improve the efficiency, seeking for new organic dye sensitizers is important. Numerous pigments such as cresyl violet [14,15], eosin-Y [16], rhodamine-6G [17], coumarin [18,19], porphyrin derivatives [20], carotenoid acids [21–23], phthalocyanines [24,25], xanthene [26,27] and squaraine [28,29], etc. are capable of ultrafast electron injection at the dye–semiconductor interface. Other directions for improving the light-to-electrical energy conversion efficiency by blocking the BET [30,31], by suppressing the density of electron-trap state at the surface of nanocrystalline semiconductor particles [9], and by controlling the degree of aggregation of adsorbed dye molecules with co-adsorbate molecules (spacers) [32–34], etc. were also reported.

Squarylium derivatives in solid forms had been considered as ideal photoconductors in building photovoltaic solar cells owing to their large extinction coefficient and broad absorption spectral range [35]. They had also been shown to be good sensitizers of colloidal TiO_2, e.g., Kamat et al. demonstrated that a squaraine is able to inject electron from its lowest singlet-excited state (S_1) into the conduction band of TiO_2 with a time constant of ~20 ps [28]. This forward ET reaction can be highly efficient because of the nanosecond lifetime of the S_1 state, the performance of charge separation, however, suffers from the BET in a subnanosecond timescale.

Ehret et al. reported a multi-pigment sensitized DSSC, for which a number of co-adsorbed cyanine dyes with high extinction coefficients and broad range of optical absorption were used [24]. Recently, Wang et al. have demonstrated the chlorophyll derivative and carotenoid co-sensitized DSSC [36]. Previously, some of the present authors showed that the light-to-electrical energy conversion efficiency of N3-sensitized DSSC could be improved by the co-adsorption with a squarylium cyanine dye in minor amount (molar ratio 1–5%), and more than 10% improvement was achieved not only in the squarylium cyanine absorption range (550–650 nm) but also in its non-absorption range (400–540 nm) [37]. The above are among few examples that utilize the multi-pigment strategy to build practical DSSC devices, and they all show significant improvement of the light-to-electrical energy conversion efficiency. In these studies, the extension of action spectrum and the optimization of redox properties among pigments have been considered as the reasons for improving the performance of DSSC [24,37]. However, a detailed mechanistic study on the charge and/or excitation energy transfer reactions involving in the co-sensitization still remains absent. Most recently, a time-resolved spectroscopic investigation on the chlorophyll derivative-carotenoid co-sensitization of nanocrystalline TiO_2 showed that carotenoid can be used as a spacer molecule to effectively reduce the radical cation of chlorophyll derivative [38]. In the present work, we have attempted to investigate the mechanism of N3 and squarylium cyanine co-sensatization of TiO_2 by means of time-resolved spectroscopies. It is shown that squarylium cyanine as a co-adsorbate functions as a sensitizer by injecting electrons into the conduction band of TiO_2 and, more importantly, as a TiO_2-to-N3 BET blocker by reducing the one-electron oxidation product $N3^{\bullet+}$. Both the lowest singlet-excited state and the ground state of the squarylium cyanine play important roles in improving the conversion efficiency.

2. Materials and methods

2.1. Sample preparation

N3 was synthesized using a previously established procedure [6]. The synthesis of 1,3-bis(*N*-3-sulphopropyl-3,3-dimethyl-2-methylene indolenine)squarylium cyanine pyridyl salt (Scheme 1; abbreviated as SQC) and its characterization are given in detail in ref. [39]. The extinction coefficient of SQC in ethanol was determined to be $\varepsilon_{632\ nm} = 2.04 \times 10^5\ M^{-1}\ cm^{-1}$. The colloidal TiO_2 particles were prepared by hydrolysis of tetrabutyl titanate in ethanol, and the average size of TiO_2 particles was about 5 nm in diameter as determined by transmission electron microscopy morphology. The stable and transparent TiO_2 colloid at a concentration of 0.05 M, without any stabilizer added, was diluted to desired concentration using absolute ethanol (pH ~3) immediately before spectroscopic measurements.

In time-resolved spectroscopic measurements, a number of preparations with different N3-to-SQC relative concentrations were used. For time-resolved fluorescence spectroscopy, the concentration of SQC was fixed at 1.6×10^{-6} M, while that of N3 was adjusted to the N3-to-SQC molar ratios of 5:1 and 50:1. For femtosecond time-resolved absorption spectroscopy, the concentration of N3 and SQC were 2.0×10^{-4} and 4.0×10^{-5} M, respectively. For both fluorescence and absorption measurements, TiO_2 was kept at 0.01 M in ethanol. By the use of Kamat's method [40] and based on our data of fluorescence quench, the apparent SQC–TiO_2 association constant was determined to be 1320 M^{-1}, and the degree of association to be ~93%.

In our previous work for the construction of practical cell devices, we used a much higher concentration of SQC (0.5×10^{-3} M) and observed the adsorption-induced formation of H-aggregation [37]. In the present work, we have intended to avoid the aggregation of SQC both free in ethanol and adsorbed on TiO_2 particle with the above diluted solution.

2.2. Time-resolved spectroscopies

For time-resolved fluorescence experiments, the excitation laser pulses at 590 nm were provided by an optical parametric amplifier (OPA-800CF, Spectra Physics) which was pumped

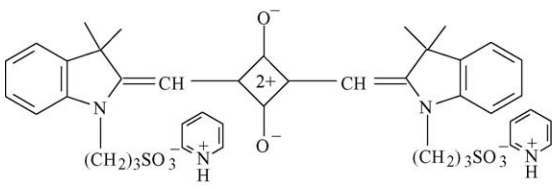

Scheme 1. Schematic structure of 1,3-bis(*N*-3-sulphopropyl-3,3-dimethyl-2-methylene indolenine)squarylium cyanine pyridyl salt (SQC).

by the output (800 nm, ~130 fs, 0.7 mJ, 1 kHz) from a regenerative amplifier (Spitfire, Spectra Physics). Fluorescence was collected and sent to a polychromator (C5094, Hamamatsu Photonics) before arriving at the photocathode of a streak camera (C2909, Hamamatsu Photonics). Time-resolved fluorescence spectra were recorded with a temporal resolution of ~30 ps and a spectral resolution of 1 nm. The excitation pulse energy was 0.1 μJ/pulse.

For time-resolved absorption measurements, the pulsed laser source was the same as that described above. The setup was based on a magic-angle pump-probe scheme in which supercontinuum probe and multichannel detection were used [41]. The time resolution of the femtosecond spectrometer was about 150 fs (full-width-at-half-maximum of the instrumental response function). The excitation pulsed energy was 0.2 μJ/pulse at 532 nm as measured at the flow-type sample cell (optical path length 1 mm). All the spectroscopic measurements were carried out at room temperature (298 K).

3. Results

3.1. Steady state spectroscopies

In the absence of N3, SQC/TiO_2 exhibits an absorption maximum at 638 nm which shifted to red for ~6 nm with respect to that of free SQC (Fig. 1, inset). This significant amount of spectral shift implies the formation of SQC–TiO_2 complex via chemical adsorption. Fig. 1 shows the absorption spectrum of N3/SQC/TiO_2 with a N3-to-SQC molar ratio of 50:1. Here again, the absorption maximum of SQC (638 nm) exhibits a 6-nm red-shift with reference to free SQC, i.e. the co-adsorption with N3 did not cause any further change of the SQC absorption. On the other hand, no N3-to-SQC singlet excitation energy transfer (EET) can be recognized from the fluorescence excitation profile, which is understandable in

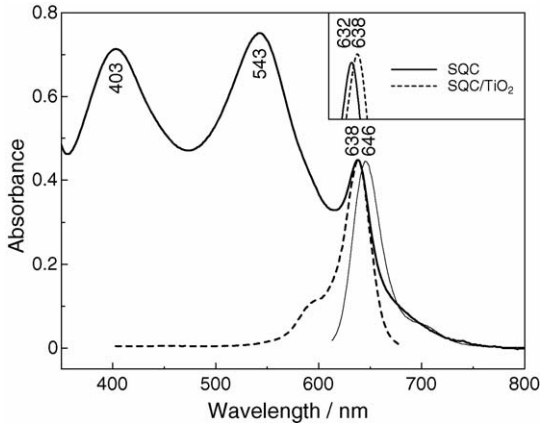

Fig. 1. Steady state absorption spectrum of N3/SQC/TiO_2 in ethanol (thicker solid line) recorded on a UV–vis spectrometer (U-3310, Hitachi), fluorescence emission spectrum (thinner solid line; λ_{exc} = 590 nm) and fluorescence excitation spectrum (broken line; λ_{obs} = 700 nm) recorded on a fluorescence spectrophotometer (F-2500, Hitachi). Inset: Absorption band peaks for SQC in ethanol (solid line) and with TiO_2 (broken line) (N3: 4.9×10^{-5} M, SQC: 1.0×10^{-6} M, TiO_2: 0.01 M).

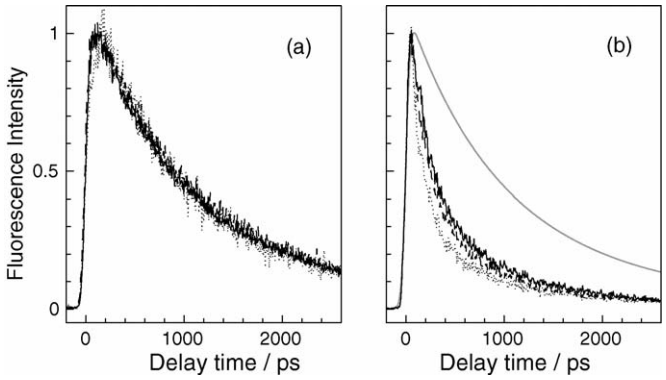

Fig. 2. Normalized fluorescence kinetics for SQC and N3 free in ethanol (a) and mixed with colloidal TiO_2 (b). In both panels, curves for SQC are shown in solid lines, N3/SQC (50/1) in dotted lines, and N3/SQC (5/1) in broken lines. In (b) the fitting curve for SQC free in ethanol is shown in light gray for comparison (λ_{exc} = 590 nm; λ_{pr} = 640 nm).

view of the extremely short-lived ^{1}MLCT* state of N3 (<100 fs) [7].

3.2. Time-resolved fluorescence spectroscopy

3.2.1. Identification of two conformers of ^{1}SQC*

When free in ethanol, the fluorescence kinetics of SQC and those of N3/SQC mixtures are almost identical (Fig. 2a), indicating that N3 did not affect the population of the emissive lowest singlet-excited state of SQC (hereafter referred to as ^{1}SQC* or S_1). For free SQC in ethanol (Fig. 3a), the fluorescence kinetics curves at 20 representative wavelengths were simultaneously fit to a bi-exponential function. The analyses yielded a longer (τ_1) and a shorter (τ_2) decay time constant as listed in Table 1, corresponding to the decay associated fluorescence spectra (DAFS) of component-1 and component-2, respectively.

It is seen in the top panel of Fig. 3a that the summation of DAFS spectra of component-1 and component-2 agrees well with the steady state fluorescence spectrum, indicating that these two components contribute predominantly to the overall fluorescence. The two DAFS components exhibit a similar full-width-at-half-maximum (~25 nm), however, component-1's peak wavelength (642 nm) is 4 nm longer than component-2's (638 nm). In addition, the kinetics behavior at the shoulder band (700 nm) and the main band (640 nm) are identical as justified by a close comparison between their kinetics traces, suggesting that these two bands originate from the same electronic state.

A solvent–effect test was made to identify the origins of the two fluorescence components. In Table 1, it is clear that on going from ethanol to ethylene glycol, the relative amplitude of component-2 decreases and eventually vanishes. This systematic change in kinetics tightly correlates to the increase of solvent viscosity and, therefore, strongly suggests the formation of a twisted ^{1}SQC* conformer following the Franck–Condon (FC) excitation. Specifically, component-2 having a shorter maximal wavelength originated from the twisted ^{1}SQC* conformer, while component-1 from the planar FC-excited conformer. Bis[4-(dimethylamino)phenyl]squaraine, as a structural analogue of SQC, was also reported to form twisted conformers after FC-

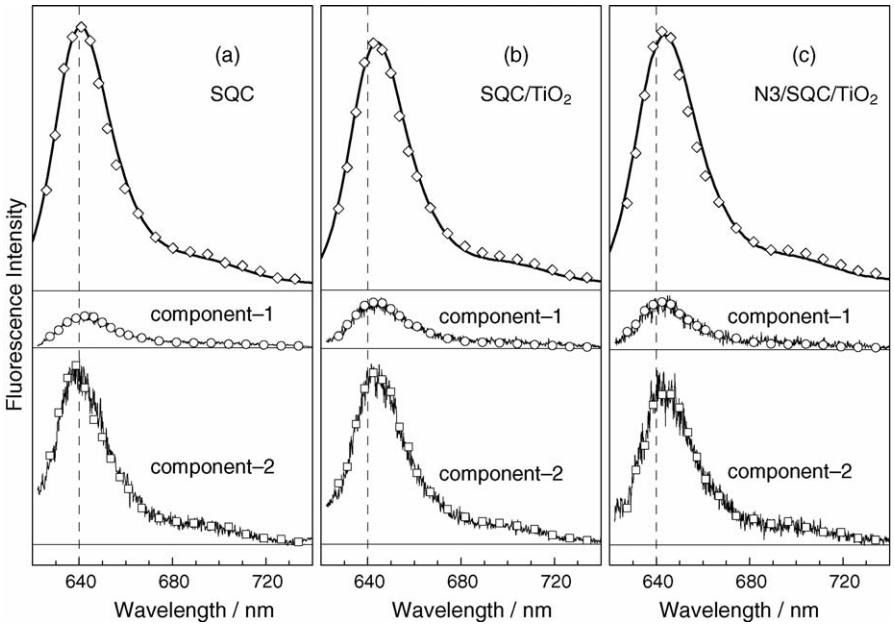

Fig. 3. Results of simultaneously fitting 20 representative kinetics traces: (a) SQC, (b) SQC/TiO_2 and (c) N3/SQC/TiO_2 (50/1) in ethanol. For each column, top panel shows the steady state fluorescence spectrum (solid line), and the summation of DAFS spectra of component-1 and component-2 (open diamond); middle panel shows the integrated spectrum in the delay time range of 2.45–2.75 ns (solid line), and the DAFS spectra of component-1 (open circle); bottom panel shows a difference spectrum obtained by subtracting the integrated spectra between delay times of 2.45–2.75 ns from that between 0.0 ns and 0.5 ns (solid line), and the DAFS spectra of component-2 (open square) (λ_{exc} = 590 nm; DAFS: decay associated fluorescence spectrum).

excitation based on spectroscopic evidence [42]. In addition, the planar and the twisted conformations of the excited-state squaric acid derivatives had been proven, both experimentally and theoretically, to be important relaxation pathways [43]. A recent theoretical work also showed that the planar form of a model squaraine is energetically stable in its S_0 state, and rapid geometrical change takes place along the potential energy surface of the S_1 state following the vertical excitation [29].

3.2.2. *Quench of ^{1}SQC* fluorescence upon adsorption on TiO_2 and co-adsorption with N3*

As shown in Fig. 2b and Table 1, upon adsorbing on colloidal TiO_2 particles the fluorescence lifetimes of ^{1}SQC* decrease drastically with reference to free SQC, i.e. from 1.67 ns to 1.04 ns and from 0.72 ns to 0.21 ns, respectively, for the planar and the twisted conformers. This is in accordance with the significant reduction of the overall fluorescence quantum yield, i.e. from 0.64 to 0.26, as measured by steady state fluorescence spectroscopy. The quench of ^{1}SQC* fluorescence is going to be attributed to the ^{1}SQC*-to-TiO_2 ET reaction. Compared to SQC free in ethanol, the adsorption on TiO_2 considerably increased the composition of component-1, i.e. from 48% to 70%, suggesting the restriction by SQC–TiO_2 interaction on the torsion freedom around the C–C bonds between the central C4-unit and the sulphonate anion groups (Scheme 1).

Compared to SQC/TiO_2, the co-adsorption of the major sensitizer N3 in N3/SQC/TiO_2 did not alter the DAFS spectra as seen by comparing Fig. 3b and c, but significantly shortened the ^{1}SQC* fluorescence lifetimes, i.e. from 1.04 ns to 0.74 ns for component-1 and 0.21–0.12 ns for component-2 (Fig. 2b; Table 1). In the absence of TiO_2, to the contrary, simply mixing N3 and SQC did not alter the SQC fluorescence lifetimes (Fig. 2a). These results imply that the co-adsorption on TiO_2

Table 1
Decay time constants (τ_i) obtained by simultaneously fitting 20 kinetics curves at selected wavelengths from the time-resolved fluorescence spectra[a]

Solvent (η (mN s/m^2))[b]	Dyes	Component-1 (τ_1 (ns))	Component-2 (τ_2 (ns))
Ethylene glycol (13.35)	SQC	1.36 (100)	—
1,2-Propanediol (11.3)	SQC	2.08 (92)	1.01 (8)
Dimethyl suphoxide (2.47)	SQC	0.84 (86)	0.30 (14)
Ethanol (1.074)	SQC	1.67 (48)	0.72 (52)
	SQC/TiO_2	1.04 (70)	0.21 (30)
	N3/SQC/TiO_2 (5/1)	0.85 (70)	0.17 (30)
	N3/SQC/TiO_2 (50/1)	0.74 (73)	0.12 (27)

The N3-to-SQC molar ratios and the relative amplitudes in percentage are given in parentheses.
[a] The model function $a_0 + a_1 \times \exp(-t/\tau_1) + a_2 \times \exp(-t/\tau_2)$ was used.
[b] Viscosity η at 25 °C taken from ref. [54].

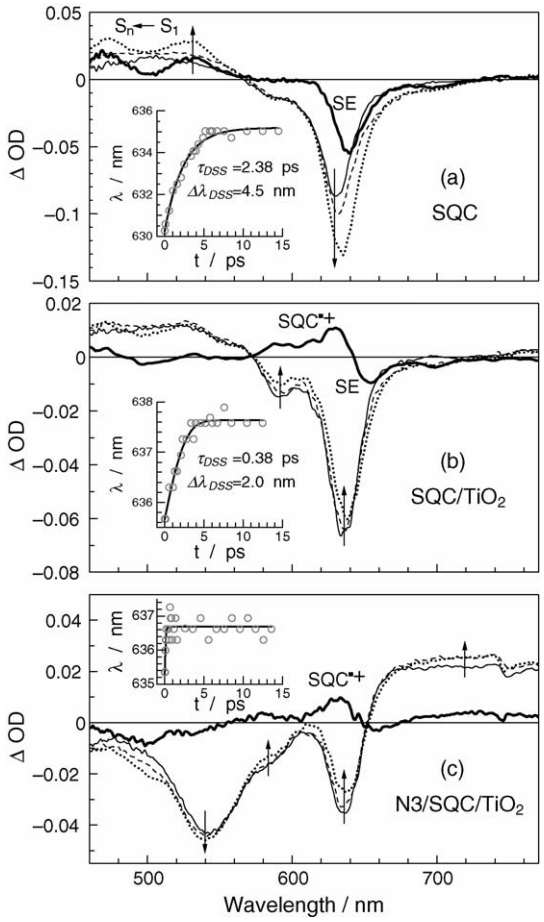

Fig. 4. Subpicosesond time-resolved absorption spectra for (a) SQC, (b) SQC/TiO_2 and (c) N3/SQC/TiO_2 at the delay times of 0.5 ps (thinner solid line), 2.0 ps (broken line) and 15.0 ps (dotted line). In each panel, a thicker solid line stands for the 15-ps-minus-0.5-ps spectrum, arrows indicate the direction of intensity evolution. Inset: Each panel shows the kinetics of the dynamic Stokes shift (DSS) of the negative band around 636 nm (N3: 2.0×10^{-4} M, SQC: 4.0×10^{-5} M, TiO_2: 0.01 M; $\lambda_{exc} = 532$ nm).

brings N3 to the close proximity of SQC molecules which results in further quench of ^{1}SQC* fluorescence.

3.3. Time-resolved absorption spectroscopy

Femtosecond time-resolved absorption measurements were carried out to study the mechanism of SQC and N3 co-sensitization of TiO_2. Fig. 4 shows the transient spectra at the delay time of 0.5 ps, 2.0 ps and 15.0 ps together with the spectra obtained by subtracting the 0.5-ps transient from the 15-ps one (thicker solid curves in each panel). The difference spectra stress the spectral features of photo-induced transient species in which the effect of bleaching of ground state absorption (BLC) is removed.

The excited-state dynamics of N3–TiO_2 in femtosecond-to-picosecond timescales had been extensively studied (see, e.g. [7,8,44]), and the squaraine–TiO_2 system was also previously examined with picosecond time-resolved absorption spectroscopy [28]. The present work emphasizes on the interplay between N3 and SQC as the co-adsorbates of TiO_2, and focuses on the excited-state dynamics of ^{1}SQC* with a much higher time resolution.

3.3.1. Assignments to the transient spectra

For SQC free in ethanol (Fig. 4a), the negative band around 640 nm exhibits apparent dynamic Stokes shift (DSS), this band originate from the $S_1 \rightarrow S_0$ stimulated emission (SE) superimposing on the negative BLC at ~632 nm. The total amount of DSS is $\Delta\lambda_{DSS} \sim 4.5$ nm which roughly coincides with the wavelength deference between the planar and the twisted ^{1}SQC* (4 nm). The inset of Fig. 4a shows the time-evolution of the peak wavelength from which a time constant of spectral equilibration was determined as $\tau_{DSS} \sim 2.38$ ps. This DSS was mainly caused by conformational relaxation of ^{1}SQC*, whereas the contribution from solvation is negligible because of the small change in dipole moment between the S_0 and the S_1 states and the rather weak photo-induced CT character confined primarily in the central C_4O_2 unit [45,46]. In parallel with DSS, the $S_n \leftarrow S_1$ excited state absorption (ESA) in the range of 460–560 nm increases and shows slight spectral narrowing, which is a clear indication of the vibrational relaxation in the S_1 state [47].

For SQC/TiO_2 (Fig. 4b), the major negative band also shows DSS but with a smaller $\Delta\lambda_{DSS}$ (~2 nm) and a much shorter time constant of spectral equilibration ($\tau_{DSS} \sim 0.38$ ps) with respect to free SQC. In the 15-ps-minus-0.5-ps spectrum, a sizable ESA appears in the region of 560–640 nm that is not seen in the case of free SQC. This new ESA signal is ascribed to $SQC^{\bullet+}$ because it closely resembles the characteristic absorption spectrum of $SQC^{\bullet+}$ reported by Kamat et al. [28]. The presence of $SQC^{\bullet+}$ clearly indicates a fast ^{1}SQC*-to-TiO_2 ET reaction, however, this does not mean a ET time constant of 15 ps: with reference to the 15-ps-minus-0.5-ps spectrum, the 2-ps-minus-0.5-ps one exhibits little $SQC^{\bullet+}$ signal, whereas the 100-ps-minus-0.5-ps one is more than two-fold stronger (data not shown), i.e. the $SQC^{\bullet+}$ population at 15 ps is still in the process of building up.

In Fig. 4c, SQC/N3/TiO_2 shows BLC signals at 590 nm and 640 nm similarly as SQC/TiO_2 does. In addition, broad and intensive signals appear in the range of 460–560 nm (negative) and 680–770 nm (positive), which are assignable to the BLC of N3 and the ESAs of N3* and/or $N3^{\bullet+}$, respectively [8]. For N3-to-TiO_2 ET reactions on a timescale longer than 0.5 ps which is the case here, ^{3}MLCT* is the predominant donor state because ^{1}MLCT* deactivates within a few tens of femtoseconds [7].

3.3.2. Analyses of the kinetics traces at selected wavelengths

In Fig. 4b for the case of SQC/TiO_2, both the 590-nm and the 640-nm BLC bands decrease due to the cancellation effect from the positive-going $SQC^{\bullet+}$ absorption, therefore, the kinetics at 590 nm and 640 nm can be used to probe the dynamics of $SQC^{\bullet+}$. In addition, the kinetics at 530 nm can be used to probe ^{1}SQC*. As for the case of N3/SQC/TiO_2 (Fig. 4c), the 750-nm trace is used to probe the transient species ^{3}N3* and/or $N3^{\bullet+}$. The negative signals in 460–540 nm increase slightly in the initial few picoseconds, according to ref. [8], this rise is due to the decay of the positive ESA from the radical anions of the dcbpy

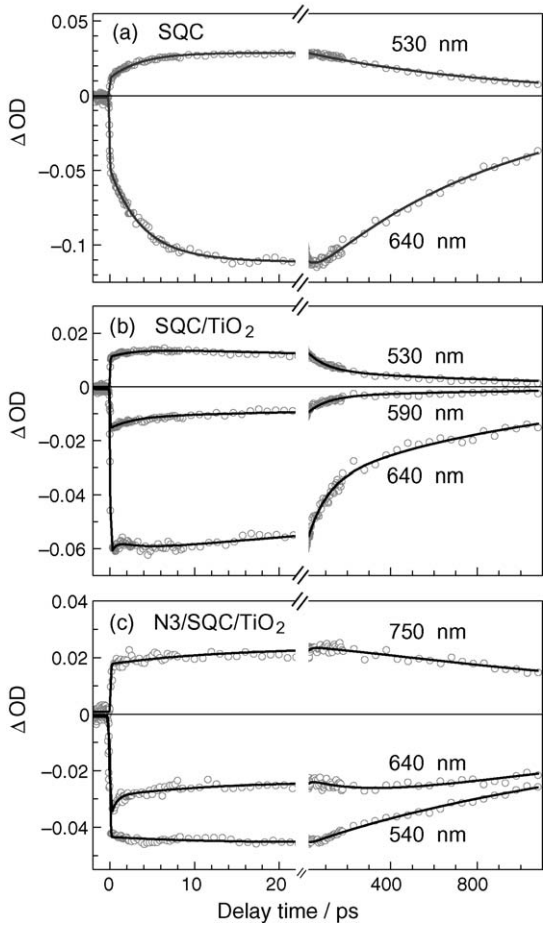

Fig. 5. Experimental kinetics traces (open circles) and fitting curves (solid lines) at the indicated wavelengths for (a) SQC, (b) SQC/TiO_2 and (c) N3/SQC/TiO_2. Kinetics traces taken from the corresponding time-resolved absorption spectra in Fig. 4. For fitting parameters see Table 2.

ligands. To trace the BET dynamics associated with the $N3^{\bullet+}$ reduction, we focus on the 540-nm BLC kinetics. The kinetics traces at selected probing wavelengths are presented in Fig. 5.

We simultaneously fit the kinetics curves to a multi-exponential model function for each case in Fig. 5, the results are listed in Table 2. The exponential components can be categorized into group-1 and group-2 according to their timescales. Although the kinetics of free SQC may obey exponential behavior, those of the other two cases do not necessarily so because of the heterogeneity of the binding forms of N3 and SQC, and because of the superposition of ESA and BLC signals. This circumstance results in considerable deviation of the time constants from those obtained by time-resolved fluorescence spectroscopy.

4. Discussion

The time-resolved spectroscopic results clearly show (i) the quench of ^{1}SQC* fluorescence upon adsorption on TiO_2 and further co-adsorption with N3 and, (ii) the formation of $SQC^{\bullet+}$ on picosecond timescales following femtosecond pulsed excitation. Hereafter, we examine the mechanism of N3 and SQC co-sensitization of TiO_2 on the basis of the above kinetics data.

Table 2
Time constants (τ_i) and amplitudes at selected probe wavelengths (λ_{pr}) derived from curve fitting to the subpicosecond kinetics in Fig. 5

Sample	λ_{pr} (nm)	Group-1		Group-2	
		τ_1 (ps)	τ_2 (ps)	τ_3 (ps)	τ_4 (ns)
SQC			$\tau_2 = 3.79$	$\tau_3 = 51.90$	$\tau_4 = 0.90$
	530		−0.018 (r)		0.029
	640		0.060 (r)	0.016 (r)	−0.120
SQC/TiO_2		$\tau_1 = 0.54$	$\tau_2 = 2.87$	$\tau_3 = 89.72$	$\tau_4 = 1.07$
	530		−0.003 (r)	0.008	0.006
	590		−0.004	−0.007	−0.003
	640	−0.007	0.005 (r)	−0.025	−0.035
N3/SQC/TiO_2[a]		$\tau_1 = 0.61$	$\tau_2 = 14.25$	$\tau_3 = 316.97$	$\tau_4 = 1.98$
	540		0.003 (r)	−0.002	−0.044
	640	−0.010	−0.006	0.014 (r)	−0.035
	750		−0.006 (r)	0.002	0.025

For each sample, kinetics traces are simultaneously fit to a summation of exponentials. "r" in parentheses denotes a rise component.
[a] N3-to-SQC molar ratio, 50:1.

4.1. The role of ^{1}SQC* in co-sensitization

For free SQC (Fig. 5a; Table 2), the longest time constant, $\tau_4 = 0.90$ ns, is not too far from an average of the amplitude-weighted lifetimes of the two fluorescent components in Table 1 (1.17 ns). The rise component τ_3 (51.9 ps) with 20% amplitude seen only in the 640-nm trace is possibly originated from the vibrational relaxation process in the ground state of SQC. Upon binding to TiO_2 (Fig. 5b; Table 2), a decay phase with $\tau_3 \sim 90$ ps is clearly seen in the kinetics trace at 530 nm for ^{1}SQC*, the same decay phase found also in the 640-nm and the 590-nm traces can be ascribed to the cancellation effect from the positive-going rise of the $SQC^{\bullet+}$ absorption. We therefore attribute this 90-ps phase to the ^{1}SQC*-to-TiO_2 ET reaction, which is responsible for the quench of ^{1}SQC* fluorescence. The longest time constant, $\tau_4 = 1.07$ ns, is very close to the fluorescence lifetime of component-1 (Table 1, 1.04 ns).

By the use of the fluorescence lifetimes in Table 1 for SQC free in ethanol and bound to TiO_2, the time constants (efficiency) of ^{1}SQC*-to-TiO_2 ET reaction for the planar and the twisted conformers are estimated to be 2.76 ns (38%) and 0.30 ns (70%), respectively. The relatively higher ET efficiency from the twisted ^{1}SQC* is in consistence with the fact that the corresponding DAFS of component-2 underwent a 4-nm bathochromic shift upon binding to TiO_2, whereas component-1 did not (Fig. 3a and b), and accordingly, the twisted conformer of ^{1}SQC* must interact stronger with TiO_2 than the planar conformer does (vide infra). The apparent difference between the ET time constants determined by transient absorption and by time-resolved fluorescence spectroscopies is due to the severe superposition of transient absorption and the complication from the kinetics mentioned before. We take the ET time constants determined by transient absorption (90 ps) and by time-resolved fluorescence (300 ps) as the lower and upper limits, respectively.

The ^{1}SQC*-to-TiO_2 ET reaction holds both structural and thermodynamical basis: the sulphonate anion groups in SQC can chelate to Ti^{4+} sites at the surface of nanocrystalline TiO_2, which is similar as the phosphonate group in a perylene-derivative chromophore [48]. In addition, the electron-rich C_4O_2 unit of SQC in ground state forms weak van der Waals interaction with the titanium center on the TiO_2 nanoparticle (leading to the SQC–TiO_2 complex), which can be significantly enhanced upon electronic excitation [29]. Energetically, the oxidation potential of ^{1}SQC* (−1.39 V versus SCE), as obtained based on the oxidation potential of SQC (0.56 V versus SCE) and the spectroscopic data, is well above the bottom of the conduction band of TiO_2 (−0.5 V versus SCE).

Compared to SQC/TiO_2, the co-adsorption of N3 resulted in a significant prolongation of the BLC kinetics at 640 nm as clearly seen in Fig. 5c and Table 2 for N3/SQC/TiO_2. This strongly suggests that it was the ET from ^{1}SQC* to $N3^{\bullet+}$ rather than the EET from ^{1}SQC* to N3 led to the additional quench of ^{1}SQC*, because the deactivation of ^{1}SQC* via EET would otherwise accelerate the recovery of the 640-nm BLC. Therefore, ^{1}SQC*-to-$N3^{\bullet+}$ ET, in addition to ^{1}SQC*-to-TiO_2 ET, is also responsible for the observed fluorescence quench of ^{1}SQC* (Fig. 2b). The time constants of ^{1}SQC*-to-$N3^{\bullet+}$ ET are 2.76 ns and 0.28 ns for the planar and the twisted conformers, respectively, as estimated on the basis of the fluorescence results in Table 1.

4.2. The role of ground state SQC in co-sensitization

An important piece of information from the femtosecond results of N3/SQC/TiO_2 (Fig. 5c; Table 2) is the identification of a 317-ps rise phase (τ_3) in the 640-nm trace, which also appears as a decay phase in either the 540-nm or the 750-nm trace. This phase is ascribed to the SQC-to-$N3^{\bullet+}$ ET reaction because it was neither found for free SQC nor for SQC/TiO_2. Here, the electron donor state of SQC must be its ground state, because ET reactions from ^{1}SQC* would not cause any apparent increase in the 640-nm BLC kinetics. Thus, the ground state SQC also plays a role in reducing $N3^{\bullet+}$. This reaction is energetically favorable in view of the redox potentials of $SQC/SQC^{\bullet+}$ (0.56 V versus SCE) and $N3/N3^{\bullet+}$ (0.85 V versus SCE), and is in accordance with our previous report on the photocurrent action spectra of the N3/SQC/TiO_2 DSSC, for which significant enhancement (>10%) of photocurrent response was observed even in the spectral range of 400–500 nm where SQC shows little optical absorption [37].

4.3. Excited state dynamics in early timescales

We now consider the early-stage spectral dynamics in Figs. 4 and 5 and the corresponding time constants of group-1 in Table 2. These time constants can hardly be correlated to the formation of $SQC^{\bullet+}$ from ^{1}SQC*, because no decay phases with similar timescales are found in the kinetics of ^{1}SQC* at 530 nm. These subpicosecond-to-picosecond timescales mainly reflect the conformational and vibrational relaxation processes in ^{1}SQC* as discussed below.

From free SQC to SQC/TiO_2 and further to N3/SQC/TiO_2 (Fig. 4, insets), λ_{DSS} and τ_{DSS} decrease, respectively, in the orders of 4.5 nm, 2.0–1.0 nm and 2.38 ps, 0.38–0.13 ps. This trend of DSS change indicates the acceleration of conformational relaxation in ^{1}SQC* upon binding to TiO_2 and further upon co-adsorption with N3, both of which restrict the conformational freedoms of ^{1}SQC*. In the case of free SQC (Fig. 5a; Table 2), the rise phase (τ_2 = 3.79 ps) in both 530-nm and 640-nm traces is attributed to the vibrational relaxation in ^{1}SQC*. Upon binding to TiO_2 (Fig. 5b; Table 2) the relaxation processes became slightly faster, i.e. shortened to 2.87 ps. In addition, the decay time constant τ_1 = 0.54 ps, found only in the 640-nm kinetics and close to that of the conformational relaxation (τ_{DSS} = 0.38 ps), reflects an apparent decay caused by the DSS of the BLC band. Finally, global kinetics analyses on N3/SQC/TiO_2 (Fig. 5c; Table 2) have identified a rise phase (τ_2 = 14.25 ps) in the 540-nm and 750-nm traces, which can be ascribed to the ^{3}MLCT*-to-TiO_2 ET reactions whose typical timescales are 1–60 ps [8]. Here, we concluded that the aforementioned ^{1}SQC*-to-TiO_2 or ^{1}SQC*-to-$N3^{\bullet+}$ ET reactions proceed from both conformationally and vibrationally relaxed ^{1}SQC* molecules.

5. Conclusion

We have investigated the mechanism of N3 and SQC co-sensitization of colloidal TiO_2 by the use of time-resolved spectroscopies. Following the subpicosecond-to-picosecond conformational and vibrational relaxation, ^{1}SQC* injects electron into the conduction band of TiO_2 in the timescale of 90–300 ps. Since this ET reaction is much slower compared to the N3-to-TiO_2 ET reaction, SQC must be a less-efficient photo-sensitizer of TiO_2. However, when it is used as a co-adsorbate of N3, both its lowest singlet-excited state and ground state can effectively regenerate N3 from $N3^{\bullet+}$, these secondary ET reactions (∼300 ps) are significantly faster than the $TiO_2(e^-)$-to-$N3^{\bullet+}$ BET reaction (μs–ms), therefore, allowing SQC to be an efficient BET interceptor. The timescale of the SQC-to-$N3^{\bullet+}$ ET reactions (∼317 ps) is also of practical significance compared to the timescale of $N3^{\bullet+}$ reduction by I^-/I_3^- electrolyte (∼10 ns [2,49] or ∼μs [36]). Practically, only an adequate minor amount of SQC can enhance the light-to-electricity conversion efficiency of the N3/SQC/TiO_2 DSSC because of the above kinetics reason and the rather narrow absorption range of SQC (550–650 nm).

The above co-sensitization mechanism readily accounts for our previous observation that SQC as a minor co-adsorbate considerably enhanced the photocurrent response of the N3/SQC/TiO_2 DSSC, i.e. more than 10% improvement in the conversion efficiency was achieved not only in the spectral region where SQC strongly absorbs light, but also in the region where it shows little absorption [36]. The recent progress in cyanine–cyanine [24,50], chlorophyll–carotenoid [36], cyanine–squaraine [51,52] and pigment–protein complex [53] co-sensitization points to a new direction for improving the performance of dye-sensitized solar cell. To construct a multi-pigment co-sensitized DSSC is in a sense to mimic a photosynthetic organism in which the pigment assembly is arranged in

an organized manner to best realize the physiological functions such as charge transfer, light harvesting and photoprotection. For the multi-pigment co-sensitization of TiO_2, a number of organic dyes with tailored excited state dynamics and redox properties can be attached or even assembled onto the surface of nanocrystalline TiO_2, which may allow, beside the sensitization of semiconductor, more functionalities for the improvement of the efficiency as well as the durability of DSSC devices. Obviously, the understanding in the mechanism of co-sensitization is of particular importance for this purpose.

Acknowledgements

This work has been jointly supported by grants from the NSFC (#90101010, #20273077, #20433010), the Major State Basic Research Development Program (G2000028204, G1998010100), and the Knowledge Innovation Program of CAS. We are grateful for the stimulating discussion with Prof. Yu-Xiang Weng at the Institute of Physics (CAS).

References

[1] B. O'Regan, M. Grätzel, Nature 353 (1991) 737–740.
[2] A. Hagfeldt, M. Grätzel, Acc. Chem. Res. 33 (2000) 269–277.
[3] K. Kalyanasundaram, M. Grätzel, Coord. Chem. Rev. 177 (1998) 347–414.
[4] M. Grätzel, Nature 414 (2001) 338–344.
[5] M. Grätzel, J. Photochem. Photobiol. A: Chem. 164 (2004) 3–14.
[6] M.K. Nazeeruddin, A. Kay, I. Rodicio, R. Humphry-Baker, E. Müller, P. Liska, N. Vlachopoulos, M. Grätzel, J. Am. Chem. Soc. 115 (1993) 6382–6390.
[7] G. Benkö, J. Kallioinen, J.E.I. Korppi-Tommola, A.P. Yartsev, V. Sundström, J. Am. Chem. Soc. 124 (2002) 489–493.
[8] J. Kallioinen, G. Benkö, V. Sundström, J.E.I. Korppi-Tommola, A.P. Yartsev, J. Phys. Chem. B 106 (2002) 4396–4404.
[9] Y. Tachibana, S.A. Haque, I.P. Mercer, J.R. Durrant, D.R. Klug, J. Phys. Chem. B 104 (2000) 1198–1205.
[10] J.B. Asbury, R.J. Ellingson, H.N. Ghosh, S. Ferrere, A.J. Nozik, T. Lian, J. Phys. Chem. B 103 (1999) 3110–3119.
[11] T.A. Heimer, E.J. Heilweil, J. Phys. Chem. B 101 (1997) 10990–10993.
[12] J.N. Clifford, E. Palomares, M.K. Nazeeruddin, R. Thampi, M. Grätzel, J.R. Durrant, J. Am. Chem. Soc. 126 (2004) 5670–5671.
[13] M.R. Waterland, D.F. Kelley, J. Phys. Chem. A 105 (2001) 4019–4028.
[14] I. Martini, G.V. Hartland, P.V. Kamat, J. Phys. Chem. B 101 (1997) 4826–4830.
[15] D. Liu, R.W. Fessenden, G.L. Hug, P.V. Kamat, J. Phys. Chem. B 101 (1997) 2583–2590.
[16] J. Moser, M. Grätzel, J. Am. Chem. Soc. 106 (1984) 6557–6564.
[17] C. Nasr, D. Liu, S. Hotchandani, P.V. Kamat, J. Phys. Chem. 100 (1996) 11054–11061.
[18] K. Hara, T. Sato, R. Katoh, A. Furube, Y. Ohga, A. Shinpo, S. Suga, K. Sayama, H. Sugihara, H. Arakawa, J. Phys. Chem. B 107 (2003) 597–606.
[19] A. Furube, R. Katoh, T. Yoshihara, K. Hara, S. Murata, H. Arakawa, M. Tachiya, J. Phys. Chem. B 108 (2004) 12583–12592.
[20] A.F. Nogueira, L.F.O. Furtado, A.L.B. Formiga, M. Nakamura, K. Araki, H.E. Toma, Inorg. Chem. 43 (2004) 396–398.
[21] F.G. Gao, A.J. Bard, L.D. Kispert, J. Photochem. Photobiol. A: Chem. 130 (2000) 49–56.
[22] J. Pan, G. Benkö, Y. Xu, T. Pascher, L. Sun, V. Sundström, T. Polívka, J. Am. Chem. Soc. 124 (2002) 13949–13957.
[23] L. Zhang, J. Yang, L. Wang, G.Z. Yang, Y.X. Weng, J. Phys. Chem. B 107 (2003) 13688–13697.
[24] A. Ehret, L. Stuhl, M.T. Spitler, J. Phys. Chem. B 105 (2001) 9960–9965.
[25] J. He, A. Hagfeldt, S.E. Lindquist, H. Grennberg, F. Korodi, L. Sun, B. Åkermark, Langmuir 17 (2001) 2743–2747.
[26] M. Hilgendorff, V. Sundström, J. Phys. Chem. B 102 (1998) 10505–10514.
[27] G. Benkö, M. Hilgendorff, A.P. Yartsev, V. Sundström, J. Phys. Chem. B 105 (2001) 967–974.
[28] P.V. Kamat, S. Das, K.G. Thomas, M.V. George, Chem. Phys. Lett. 178 (1991) 75–79.
[29] M.J. Paterson, L. Blancafort, S. Wilsey, M.A. Robb, J. Phys. Chem. A 106 (2002) 11431–11439.
[30] J. Krüger, R. Plass, L. Cevey, M. Piccirelli, M. Grätzel, Appl. Phys. Lett. 79 (2001) 2085–2087.
[31] A. Kay, M. Grätzel, Chem. Mater. 14 (2002) 2930–2935.
[32] K. Hara, H. Sugihara, Y. Tachibana, A. Islam, M. Yanagida, K. Sayama, H. Arakawa, Langmuir 17 (2001) 5992–5999.
[33] Y. Amao, T. Komori, Langmuir 19 (2003) 8872–8875.
[34] P. Wang, S.M. Zakeeruddin, R. Humphry-Baker, M. Grätzel, Chem. Mater. 16 (2004) 2694–2696.
[35] V.Y. Merritt, IBM J. Res. Dev. 22 (1978) 353.
[36] X.F. Wang, J.F. Xiang, P. Wang, Y. Koyama, S. Yanagida, Y. Wada, K. Hamada, S. Sasaki, H. Tamiaki, Chem. Phys. Lett. 408 (2005) 409–414.
[37] D. Zhang, W. Wang, Y. Liu, X. Xiao, W. Zhao, B. Zhang, Y. Cao, J. Photochem. Photobiol. A: Chem. 135 (2000) 235–240.
[38] X.F. Wang, Y. Kakitani, J. Xiang, Y. Koyama, F.S. Rondonuwu, H. Nagae, S. Sasaki, H. Tamiaki, Chem. Phys. Lett. 416 (2005) 229–233.
[39] W. Zhao, Y.J. Hou, X.S. Wang, B.W. Zhang, Y. Cao, R. Yang, W.B. Wang, X.R. Xiao, Sol. Energy Mater. Sol. Cells 58 (1999) 173–183.
[40] P.V. Kamat, J.P. Chauvet, R.W. Fessenden, J. Phys. Chem. 90 (1986) 1389–1394.
[41] R.M. Han, Y.S. Wu, J. Feng, X.C. Ai, J.P. Zhang, L.H. Skibsted, Photochem. Photobiol. 80 (2004) 326–333.
[42] K.Y. Law, J. Phys. Chem. 91 (1987) 5184–5193.
[43] C. Gude, W. Rettig, J. Phys. Chem. A 104 (2000) 8050–8057.
[44] J.N. Clifford, E. Palomares, M.K. Nazeeruddin, M. Grätzel, J. Nelson, X. Li, N.J. Long, J.R. Durrant, J. Am. Chem. Soc. 126 (2004) 5225–5233.
[45] R.W. Bigelow, H.-J. Freund, Chem. Phys. 107 (1986) 159–174.
[46] The Stokes shift, defined as the difference between fluorescence and absorption maximal wavelengths, keeps almost constant (9–10 nm) over a number of solvents with a variety of polarity and polarizability (dimethyal sulphoxide, *N*,*N*-dimethylformaide, ethylene glycol, 1,2-propanediol, ethanol, methanol and water).
[47] Y. Hirata, T. Okada, Chem. Phys. Lett. 187 (1999) 203–207.
[48] B. Burfeindt, T. Hannappel, W. Storck, F. Willig, J. Phys. Chem. 100 (1996) 16463–16465.
[49] T.A. Heimer, E.J. Heilweil, C.A. Bignozzi, G.J. Meyer, J. Phys. Chem. A 104 (2000) 4256–4262.
[50] M. Guo, P. Diao, Y.J. Ren, F. Meng, H. Tian, S.M. Cai, Sol. Energy Mater. Sol. Cells 88 (2005) 23–35.
[51] K. Sayama, S. Tsukagoshi, T. Mori, K. Hara, Y. Ohga, A. Shinpou, Y. Abe, S. Suga, H. Arakawa, Sol. Energy Mater. Sol. Cells 80 (2003) 47–71.
[52] Y. Chen, Z. Zeng, C. Li, W. Wang, X. Wang, B. Zhang, New J. Chem. 29 (2005) 773–776.
[53] R. Das, P.J. Kiley, M. Segal, J. Norville, A.A. Yu, L. Wang, S.A. Trammell, L.E. Reddick, R. Kumar, F. Stellacci, N. Lebedev, J. Schnur, B.D. Bruce, S. Zhang, M. Baldo, Nano Lett. 4 (2004) 1079–1083.
[54] J.A. Dean, Lange's Handbook of Chemistry, 14th ed., McGraw-Hill Publishers, Inc., New York, USA, 1992.